

### Activity trends of binary silver alloy nanocatalysts for oxygen reduction reaction in alkaline media

Wu, Xiaoqiang; Chen, Fuyi; Zhang, Nan; Lei, Yimin; Jin, Yachao; Qaseem, Adnan; Johnston, Roy

DOI:

[10.1002/smll.201603387](https://doi.org/10.1002/smll.201603387)

License:

None: All rights reserved

*Document Version*

Peer reviewed version

*Citation for published version (Harvard):*

Wu, X, Chen, F, Zhang, N, Lei, Y, Jin, Y, Qaseem, A & Johnston, RL 2017, 'Activity trends of binary silver alloy nanocatalysts for oxygen reduction reaction in alkaline media', *Small*, vol. 13, no. 15, 1603387. <https://doi.org/10.1002/smll.201603387>

[Link to publication on Research at Birmingham portal](#)

#### **Publisher Rights Statement:**

This is the peer reviewed version of the following article: X. Wu, F. Chen, N. Zhang, Y. Lei, Y. Jin, A. Qaseem, R. L. Johnston, *Small* 2017, 13, which has been published in final form at <http://dx.doi.org/10.1002/smll.201603387>. This article may be used for non-commercial purposes in accordance with Wiley Terms and Conditions for Self-Archiving.

Uploaded 10/5/2017

#### **General rights**

Unless a licence is specified above, all rights (including copyright and moral rights) in this document are retained by the authors and/or the copyright holders. The express permission of the copyright holder must be obtained for any use of this material other than for purposes permitted by law.

- Users may freely distribute the URL that is used to identify this publication.
- Users may download and/or print one copy of the publication from the University of Birmingham research portal for the purpose of private study or non-commercial research.
- User may use extracts from the document in line with the concept of 'fair dealing' under the Copyright, Designs and Patents Act 1988 (?)
- Users may not further distribute the material nor use it for the purposes of commercial gain.

Where a licence is displayed above, please note the terms and conditions of the licence govern your use of this document.

When citing, please reference the published version.

#### **Take down policy**

While the University of Birmingham exercises care and attention in making items available there are rare occasions when an item has been uploaded in error or has been deemed to be commercially or otherwise sensitive.

If you believe that this is the case for this document, please contact [UBIRA@lists.bham.ac.uk](mailto:UBIRA@lists.bham.ac.uk) providing details and we will remove access to the work immediately and investigate.

DOI: 10.1002/ ((please add manuscript number))

**Article type: Full Paper**

**Activity Trends of Binary Silver Alloy Nanocatalysts for Oxygen Reduction Reaction in Alkaline Media**

*Xiaoqiang Wu,<sup>[a]</sup> Fuyi Chen,<sup>\*,[a]</sup> Nan Zhang,<sup>[a]</sup> Yimin Lei,<sup>[a]</sup> Yachao Jin,<sup>[a]</sup> Adnan Qaseem,<sup>[a]</sup> and Roy L. Johnston<sup>[b]</sup>*

X.Q. Wu, F.Y. Chen, N. Zhang, Y.M. Lei, Y.H. Jin, A. Qaseem,  
State Key Laboratory of Solidification Processing, Northwestern Polytechnical University,  
Xian, 710072, China  
E-mail: fuyichen@nwpu.edu.cn (Fuyi Chen)

Roy L. Johnston  
Department of Chemistry, University of Birmingham, Birmingham, B15 2TT, U.K.

**Key words:** Ag-based alloy; oxygen reduction; electronic structure; d-band centre; electrocatalysts

**Abstract:** The electrocatalytic activity of Pt-based alloys exhibits a strongly dependence on their electronic structures, but a relationship between electronic structure and oxygen reduction reaction (ORR) activity in Ag-based alloys is still not clear. Here, a vapor deposition based approach is reported for the preparation of  $\text{Ag}_{75}\text{M}_{25}$  (M=Cu, Co, Fe and In ) and  $\text{Ag}_x\text{Cu}_{100-x}$  (x=0, 25, 45, 50, 55, 75, 90 and 100) nanocatalysts and their electronic structures are determined by valence band spectra. The relationship of the d-band centre and ORR activity exhibits volcano-shape behaviors, where the maximum catalytic activity obtained for  $\text{Ag}_{75}\text{Cu}_{25}$  alloys. The ORR enhancement of  $\text{Ag}_{75}\text{Cu}_{25}$  alloys originates from the 0.12eV upshift in d-band center relative to pure Ag, which is different from the downshift in the d-band center in Pt-based alloys. The activity trend for these  $\text{Ag}_{75}\text{M}_{25}$  alloys is in the order

of  $\text{Ag}_{75}\text{Cu}_{25}$  >  $\text{Ag}_{75}\text{Fe}_{25}$  >  $\text{Ag}_{75}\text{Co}_{25}$ . These results provide an insight to understand the activity and stability enhancement of  $\text{Ag}_{75}\text{Cu}_{25}$  and  $\text{Ag}_{50}\text{Cu}_{50}$  catalysts by alloying.

## 1. Introduction

The oxygen reduction reaction (ORR) is critical for alkaline fuel cells and metal-air batteries, Pt and Pt-based alloys are known as the most efficient catalysts for ORR, however, their cost and scarcity in the earth crust have hampered their extensive application.<sup>[1]</sup> To make ORR catalysts more economical and viable, there are many problems that should be solved. The main one is to find a low cost and highly active catalyst to substitute Pt. Silver has been known as an inexpensive catalyst which could achieve this goal because of its acceptable catalytic activity, high stability in alkaline solution and low cost (about 50 times less expensive than Pt).<sup>[2]</sup> However, the rational screening of inexpensive, stable and efficient Ag-based electrocatalysts requires the understanding of the catalysis mechanisms, catalytic behavior and intrinsic effect (such as electronic effect) of these catalysts in ORR process.<sup>[3]</sup>

Recently, our group reported that the electronic perturbation to play a key role on activity and stability of Ag-Cu metallic glass electrocatalysts with performance comparable to Pt/C for zinc-air batteries.<sup>[4]</sup> Similarly Nørskov *et al.* identified the electronic effect as a factor which determined the ORR activity order of Pt-based alloys and provided a basis for the future optimal design of active and stable Pt-based catalysts.<sup>[5]</sup> But to the best of our knowledge, the ORR activity order has been rarely reported for Ag-based alloys. To this end, in 2014, Holewinski *et al.* reported the Ag-Co alloy had an excellent ORR performance, where the subsurface Co atoms provided the electronic perturbation or ligand effect, reaching up to almost half ORR activity of Pt at 0.8  $V_{\text{RHE}}$  in alkaline media.<sup>[6]</sup> From the theoretical calculations on the Ag-Co near surface alloy (NSA), the free energy diagram for ORR on the (111) surface of binary  $\text{Ag}_{75}\text{M}_{25}$  (M=Cu, Co and Fe) alloys were studied and a activity order is obtained as Pt > Ag-Fe > Ag-Co > Ag-Cu > Ag. Nevertheless, this theoretical activity order

1 is still short of the direct experimental support and is not considering the contribution of other  
2 surface, such as, the (311), (200)/(100) and (220)/(110) facets, which are suggested to be  
3  
4 more suitable for ORR in Ag-based and Pt-based alloys.<sup>[7]</sup> Yi et al. reported the activity order  
5  
6 of binary silver-based nanocatalysts supported on carbon nanotube (CNT) for ORR in alkaline  
7  
8 media,<sup>[8]</sup> it is reported that the activity of Ag-based alloys is in order of  $\text{Ag}_8\text{Co}_2/\text{CNT} >$   
9  
10  $\text{Ag}_9\text{Cu}_1/\text{CNT} > \text{Ag}/\text{CNT}$ , and the activity of  $\text{Ag}_9\text{Cu}_1/\text{CNT}$  is severely deteriorated after a  
11  
12 single polarization test on rotating disk electrode at 1600 rpm, suggesting a very low ORR  
13  
14 stability. On the contrary, the theoretical calculations from Kim et al. <sup>[3b, 9]</sup> and our group<sup>[10]</sup>  
15  
16 reported that Ag-Cu alloy nanocatalysts possess higher ORR activity and stability than pure Ag.  
17  
18 Our recent experimental work also shows that Ag-Cu alloy catalyst has good activity and  
19  
20 stability for ORR in alkaline media and presents excellent cyclic performance during  
21  
22 charging-discharging in real zinc-air batteries. <sup>[11]</sup> It is well-known that CNTs are active for  
23  
24 ORR in alkaline media, so the activity order of Ag-based alloys supported on CNT is not a  
25  
26 realistic portrayal of the alloying effect in Ag catalyst.<sup>[12]</sup> It can be inferred that the present  
27  
28 ORR activity order obtained from the (111) facets of Ag-M alloys <sup>[6]</sup> or from CNT-supported  
29  
30 Ag-M alloys <sup>[8]</sup> may be different with the real Ag-based alloys.

31  
32  
33  
34  
35  
36  
37  
38  
39 Herein, we directly deposited the  $\text{Ag}_{75}\text{M}_{25}$  (M=Cu, Co, In and Fe) and  $\text{Ag}_x\text{Cu}_{100-x}$  (x= 0,  
40  
41 25, 45, 50, 55, 75, 90 and 100) alloys on glassy carbon electrode via pulsed laser deposition  
42  
43 (PLD) and measured their activity order via rotating disk electrode (RDE) polarization test.  
44  
45 As a function of electronic perturbation in ORR, a volcano curve (specific activity vs. d-band  
46  
47 center ) for Ag-based catalysts was built and a activity order of these alloys was obtained.  
48  
49 This volcano curve provides guidance for the screening of Ag alloy catalysts, explains the  
50  
51 enhancement effects from the electronic perturbation, and provides new insight into the  
52  
53 design of alkaline fuel cells and metal-air batteries.  
54  
55  
56  
57  
58  
59  
60

## 61 2. Results and discussion

## 2.1. The ORR activity of the Ag<sub>75</sub>M<sub>25</sub> and Ag<sub>x</sub>Cu<sub>100-x</sub> alloys

**Figure 1a** and **Figure S2** show the RDE polarization curves of Ag<sub>75</sub>M<sub>25</sub> alloys measured in an O<sub>2</sub>-saturated 0.1 M KOH, **Table 1** list their ORR activities. The Ag<sub>75</sub>M<sub>25</sub> alloys demonstrate their catalytic activity changes via alloying Ag with the M elements, the half-potentials are in the order as: Pt/C-20% (0.88V<sub>RHE</sub>) > Ag<sub>75</sub>Cu<sub>25</sub> (0.76V<sub>RHE</sub>) > Ag<sub>75</sub>Fe<sub>25</sub> (0.73V<sub>RHE</sub>) > Ag<sub>75</sub>Co<sub>25</sub> (0.70V<sub>RHE</sub>) > Ag (0.66V<sub>RHE</sub>) > Ag<sub>75</sub>In<sub>25</sub> (0.56V<sub>RHE</sub>), indicating that the ORR activity of Ag is significantly changed by alloying with M (M=Co, Fe and Cu) metals. Further more, we consider the effect of amount of alloying element by carrying out activity measurements for different amount of Cu in Ag<sub>x</sub>Cu<sub>100-x</sub> alloys (see **Figure 1a**, **Figure S3** and **Table 1**). By tuning the composition of Cu, the half-wave potential of Ag<sub>x</sub>Cu<sub>100-x</sub> alloys showed a pattern of normal distribution, indicating the ORR activity is tuned by content of Cu. However, if the content of Cu become extremely high, the half-wave potential decreases because the excessive Cu atoms would occupy the position of Ag and decreases the activity site. In Cu contents ranging 0 to 50 at%, the activity of Ag<sub>x</sub>Cu<sub>100-x</sub> alloys is improved with increasing of Cu content, alloying effect play a positive role. In the Cu contents higher than 50%, the activity of Ag<sub>x</sub>Cu<sub>100-x</sub> alloys is decreased with increasing of Cu content.

The corresponding Koutecky-Levich (K-L) plots at 0.3V<sub>RHE</sub> electrode potential shown in **Figure S4** are used to evaluate the transferred electron number per oxygen molecule in ORR. The K-L plots for Ag<sub>x</sub>Cu<sub>100-x</sub> and Ag<sub>75</sub>M<sub>25</sub> catalysts display good linearity. The n values for Ag<sub>75</sub>M<sub>25</sub> (M=Cu, Co and Fe ) catalysts as calculated by K-L equations at 0.30 V<sub>RHE</sub> is 3.86, 3.82 and 3.84 respectively, demonstrating an apparent quasi-four-electron process in the Ag<sub>75</sub>M<sub>25</sub> catalyst.<sup>[13]</sup> For Ag<sub>x</sub>Cu<sub>100-x</sub> (x=0, 25, 45, 50, 55, 75, 90 and 100) alloys, the highest electron transfer number value at 0.30 V<sub>RHE</sub> is 3.97 for x=50, indicating that Ag<sub>50</sub>Cu<sub>50</sub> alloy catalysts favor four-electron reduction process.

To further determine the activity order of Ag<sub>75</sub>M<sub>25</sub> and Ag<sub>x</sub>Cu<sub>100-x</sub> alloys, we considered the specific activity and Tafel slopes of them. **Figure 1b** shows that the

1 corresponding specific activity (SA) and mass specific activity (MA) curves of these alloys in  
 2 ORR polarization test at 0.85V<sub>RHE</sub>. Both SA and MA results indicate that the Ag<sub>75</sub>Cu<sub>25</sub> alloy  
 3  
 4 (0.85 mA cm<sup>-2</sup> and 89.5 A g<sub>total</sub><sup>-1</sup>) is the most ORR active alloy among Ag<sub>75</sub>M<sub>25</sub> alloys, and  
 5  
 6 Ag<sub>50</sub>Cu<sub>50</sub> alloy (1.57 mA cm<sup>-2</sup> and 207.5 A g<sub>total</sub><sup>-1</sup>) is the most ORR active composition among  
 7  
 8 Ag<sub>x</sub>Cu<sub>100-x</sub> alloys. For refining these results, we considered the corresponding electrochemical  
 9  
 10 surface areas (ECSA) of these Ag<sub>75</sub>M<sub>25</sub> and Ag<sub>x</sub>Cu<sub>100-x</sub> alloys as present in **Figure 1c**, **Figure**  
 11  
 12 **S5** and **Table 1**. The ECSA of pure Ag (14.05 m<sup>2</sup> g<sub>total</sub><sup>-1</sup>) is lower than that of Ag-M alloys  
 13  
 14 ( range from 15.22 g<sub>total</sub><sup>-1</sup> to 16.49 g<sub>total</sub><sup>-1</sup>), suggesting a lower specific surface area of Ag  
 15  
 16 catalyst(see **Table S1**). But for Ag-M alloys, the ECSA is almost the same. This result is in  
 17  
 18 agreement with the TEM results (support information in Part 4), in which the pure Ag  
 19  
 20 nanoparticles are bigger than that of Ag-M alloys and results a lower ECSA. Using the  
 21  
 22 polarization curves of **Figure 1a**, the Tafel slopes (*K*) were observed for ORR on these  
 23  
 24 Ag<sub>x</sub>Cu<sub>100-x</sub> and Ag<sub>75</sub>M<sub>25</sub> alloys. As shown in **Figure 1d** and **Table 1**, after alloying with other  
 25  
 26 metals, the Tafel slopes in the low overpotential range is in the order of Ag<sub>75</sub>Cu<sub>25</sub>(72 mV dec<sup>-1</sup>)  
 27  
 28 <sup>1</sup>) < Ag<sub>75</sub>Fe<sub>25</sub>(76mV dec<sup>-1</sup>)< Ag<sub>75</sub>Co<sub>25</sub>(78 mV dec<sup>-1</sup>)< Ag<sub>75</sub>In<sub>25</sub>(81mV dec<sup>-1</sup>). This result is in  
 29  
 30 concomitant with the orders of specific activity and mass activity. For Ag<sub>x</sub>Cu<sub>100-x</sub> alloys, the  
 31  
 32 Tafel slope in the low overpotential range increases with the increasing of Cu content (range  
 33  
 34 from 0 to 50%) as Ag (79 mV dec<sup>-1</sup>) < Ag<sub>90</sub>Cu<sub>10</sub> (78 mV dec<sup>-1</sup>) < Ag<sub>75</sub>Cu<sub>25</sub> (72 mV dec<sup>-1</sup>) <  
 35  
 36 Ag<sub>55</sub>Cu<sub>45</sub> (69 mV dec<sup>-1</sup>). When the Cu content is higher than 50%, the Tafel slopes increase  
 37  
 38 with the increasing of Cu-content as Ag<sub>50</sub>Cu<sub>50</sub> (64 mV dec<sup>-1</sup>) < Ag<sub>45</sub>Cu<sub>55</sub> (66 mV dec<sup>-1</sup>) <  
 39  
 40 Ag<sub>25</sub>Cu<sub>75</sub> (75 mV dec<sup>-1</sup>). Here, the Ag<sub>50</sub>Cu<sub>50</sub> exhibits smallest Tafel slope and is therefore the  
 41  
 42 most efficient ORR catalyst among all the catalysts in this study, suggesting an outstanding  
 43  
 44 intrinsic ORR kinetics of Ag<sub>50</sub>Cu<sub>50</sub> alloy. Meanwhile, the better ORR catalytic activity of  
 45  
 46 Ag<sub>50</sub>Cu<sub>50</sub> alloy compared to other Ag<sub>x</sub>Cu<sub>100-x</sub> (x= 25, 45, 55, 75, 90) alloys catalysts  
 47  
 48 demonstrated that the content of Cu plays an important role in determining the ORR pathway.  
 49  
 50  
 51  
 52  
 53  
 54  
 55  
 56  
 57  
 58  
 59  
 60  
 61  
 62  
 63  
 64  
 65

## 2.2. The d-band center of the Ag<sub>75</sub>M<sub>25</sub> and Ag<sub>x</sub>Cu<sub>100-x</sub> alloys

As mentioned above, the alloying of Ag with M (Co, Fe, Cu and In) significantly changes the catalytic activity of Ag, the question arises as to why the catalytic property can be tuned by chemical composition. Considering that Pt-based alloys employ the d-band center to address this question and the role of electronic perturbation has been justified<sup>[5]</sup>, the valence band spectra (VBS) of various Ag<sub>75</sub>M<sub>25</sub> alloys were measured by high-resolution X-ray photoelectron spectroscopy (XPS). **Figure 2a** show the VBS spectra of the pure Ag and Ag<sub>75</sub>M<sub>25</sub> alloys, and **Table 2** listed the d-band center of VBS. It is shown that the surface electronic structure of Ag<sub>75</sub>M<sub>25</sub> alloys is different from that of pure Ag, which possesses an innate d-band center at -5.28eV. This d-band center of Ag coincides with the results of Timo Hofmann et al.<sup>[3a]</sup> Careful inspection of the VBS in **Figure 2a** reveals that the density of states (DOS) of Ag<sub>75</sub>M<sub>25</sub> (Co, Fe and Cu) alloys present a clearly discernible increase near the Fermi level, that is, the position of d-band center is upshifted relative to pure Ag. But for Ag<sub>75</sub>In<sub>25</sub>, the DOS is increased in the far end of VBS which leads to a downshift of d-band center to -5.51eV. Hence, the M (Cu, Co, Fe and In) elements modulate the electronic structure and affect ORR activity of Ag in Ag<sub>75</sub>M<sub>25</sub> alloys.

To obtain the further insight of the d-band center of Ag<sub>75</sub>M<sub>25</sub> alloys, the density functional theory (DFT) calculations are performed on pure Ag, Ag<sub>75</sub>Cu<sub>25</sub>, Ag<sub>75</sub>Co<sub>25</sub>, Ag<sub>75</sub>Fe<sub>25</sub> and Ag<sub>75</sub>In<sub>25</sub> (Details of model and calculation methods are shown in the Supporting Information.). As present in **Figure S6** and **Table S2**, after alloying with the M with the exception of In element, the density of state (DOS) near Fermi level of Ag<sub>75</sub>M<sub>25</sub> alloys, between 1eV and 2.5eV, present a clearly discernible increase with addition of Cu, Fe and Cu elements. The change of the d-band centers is in the order as: AgIn(-4.65eV) < Ag(-4.61eV) < AgCu(-4.51eV) < AgFe(-4.41eV) < AgCo(-4.34eV). Although the calculated d-band center from DFT is different from the experimental d-band centers from VBS, the trends of d-band center change and the increasing of DOS near Fermi level between 0 and -2.5 eV are coincide

with the experimental XPS results in **Figure 2a and 2c**, demonstrating the electronic perturbation plays a critical role on the d-band center of the  $\text{Ag}_{75}\text{M}_{25}$  alloys.

As shown in **Figure 1a**, the ORR activity of  $\text{Ag}_x\text{Cu}_{100-x}$  alloys depend on the Cu content. To explore the overall consequence of both the alloying element M and the content of M with the aim to create a more efficient catalyst than pure Ag, we considered the effects of Cu content on VBS of the  $\text{Ag}_x\text{Cu}_{100-x}$  alloys. **Figure 2b** present the VBS spectra of the pure Ag and  $\text{Ag}_x\text{Cu}_{100-x}$  alloys. As present, the degree of alloying significantly affected the VBS of  $\text{Ag}_x\text{Cu}_{100-x}$  alloys. The DOS near Fermi level, between 1eV and 3eV, is increased with the increasing of Cu content (at.%) in  $\text{Ag}_x\text{Cu}_{100-x}$  alloys, which indicates that the position of d-band tend to upshift along with the increasing Cu content.

### 2.3 The volcano curve for the $\text{Ag}_{75}\text{M}_{25}$ and $\text{Ag}_x\text{Cu}_{100-x}$ alloys

These d-band centers of VBS allow us to directly correlate the variations in the ORR catalytic activity with the alloying element variations in  $\text{Ag}_{75}\text{M}_{25}$  alloys. **Figure 2c** indicates that the d-band center of  $\text{Ag}_{75}\text{M}_{25}$  versus the specific activity at  $0.85\text{V}_{\text{RHE}}$  exhibit a volcano curve. After alloying with M (Cu, Co and Fe) metallic element, all of the d-band center of  $\text{Ag}_{75}\text{M}_{25}$  alloys are upshifted relative to pure Ag while the ORR activity of Ag catalyst is modified by alloying with M (Cu, Co and Fe) metals. Nevertheless, the relationship of d-band center and ORR activity in  $\text{Ag}_{75}\text{M}_{25}$  alloys is not merely a linear one. Here, the d-band center of  $\text{Ag}_{75}\text{Cu}_{25}$ ,  $\text{Ag}_{75}\text{Fe}_{25}$  and  $\text{Ag}_{75}\text{Co}_{25}$  is at -5.16 eV, -4.71 eV and -4.45 eV, respectively, whereas their ORR specific activity is  $0.23 \text{ mA cm}^{-2}$ ,  $0.177 \text{ mA cm}^{-2}$  and  $0.112 \text{ mA cm}^{-2}$ , respectively, indicating that the ORR activity decreases when the position of the d-band center of  $\text{Ag}_{75}\text{M}_{25}$  becomes extremely close to the Fermi energy, due to that the higher binding energy of OCS (oxygen containing species, such as  $\text{O}_2$ ,  $\text{OH}^-$ ,  $\text{OOH}^-$ ) on Ag surface which blocks the catalytic active site on the surface.<sup>[5a, 5b]</sup> But for  $\text{Ag}_{75}\text{In}_{25}$  alloy, the downshift of d-band center decreases the binding energy of Ag-OCS which would weaken the ORR activity of Ag.<sup>[5a, 5b]</sup> This leads to the maximum possible catalytic activity obtained for



1 the Ag<sub>75</sub>Cu<sub>25</sub> alloy, which binds the OCS neither too weakly nor too strongly, indicating a  
2 balance between the adsorption energies of reactive intermediates and surface coverage by  
3 blocking species. It is interesting to note that, the ORR enhancement of Ag<sub>75</sub>M<sub>25</sub> alloys  
4 originates from the upshift in d-band center and the upshift amount in d-band center of the  
5 most active Ag<sub>75</sub>Cu<sub>25</sub> is about 0.12eV relative to pure Ag, but for Pt-M alloys, the ORR  
6 enhancement comes from the downshift in the d-band center, for example, the d-band center  
7 of the most active Pt-Y,<sup>[5a, 14]</sup> Pt-Co alloy<sup>[15]</sup> and Pt-Ni alloy<sup>[16]</sup> downshifts relative to pure Pt  
8 about 0.14eV, 0.20eV and 0.19 eV, respectively, indicating that the tuning of the catalytic  
9 enhancement via electronic perturbation in Ag-M alloys is opposite to that of Pt-M alloys.  
10  
11  
12  
13  
14  
15  
16  
17  
18  
19  
20  
21

22 As shown in **Figure 2d**, the relationship between the specific activity at 0.85V<sub>RHE</sub> and the  
23 d-band center positions on Ag<sub>x</sub>Cu<sub>100-x</sub> alloys exhibits a volcano shape too, with the maximum  
24 catalytic activity obtained for Ag<sub>50</sub>Cu<sub>50</sub> (1.57 mAcm<sup>-2</sup>), indicating that ORR activity of  
25 Ag<sub>x</sub>Cu<sub>100-x</sub> alloys is depends on the alloying degree and the position of d-band states relative  
26 to Fermi level. In Cu content range lower than 50 at%, the ORR activity of Ag<sub>x</sub>Cu<sub>100-x</sub> alloys  
27 increases with the upshifting of d-band center, which enhances the Ag-OCS bond interaction  
28 and the ORR activity.<sup>[3b]</sup> For high Cu content regime ( higher than 50%), the ORR activity of  
29 Ag<sub>x</sub>Cu<sub>100-x</sub> alloys exhibit a significant decrease from 1.57 mA cm<sup>-2</sup> to 0.55 mA cm<sup>-2</sup> with  
30 increasing Cu content. Further study of XPS surface composition analysis indicates that the  
31 content of Cu is 72.11% on the surface of Ag<sub>25</sub>Cu<sub>75</sub> alloys and these excess surface Cu atoms  
32 get easily oxidized in alkaline solution, which lead to higher dissociation energy for ORR,  
33 block the activation site of the Ag atoms, and decrease the ORR activity of Ag<sub>x</sub>Cu<sub>100-x</sub>  
34 alloys.<sup>[3b]</sup> The ORR activity of Ag<sub>50</sub>Cu<sub>50</sub> is at the top of volcano curve and suggests that this  
35 alloy composition has the best balance of the d-band center and surface active site of Ag,  
36 which renders it the highest activity for ORR among all compositions.  
37  
38  
39  
40  
41  
42  
43  
44  
45  
46  
47  
48  
49  
50  
51  
52  
53  
54  
55  
56  
57  
58  
59  
60  
61  
62  
63  
64  
65

## 2.4. The typical microstructure and activity order of the Ag<sub>75</sub>M<sub>25</sub> alloys

As measured above, the activity order of these Ag<sub>75</sub>M<sub>25</sub> alloys (Ag<sub>75</sub>Cu<sub>25</sub> > Ag<sub>75</sub>Fe<sub>25</sub> > Ag<sub>75</sub>Co<sub>25</sub>) in this work is different with the activity order predicted from the (111) surface (Ag<sub>75</sub>Fe<sub>25</sub> > Ag<sub>75</sub>Co<sub>25</sub> > Ag<sub>75</sub>Cu<sub>25</sub>).<sup>[6]</sup> To evaluate this argument, we measured the surface characters of these alloys. **Figure 3a** and **Figure S7** present the typical microstructure of these as-prepared catalysts measured by high resolution transmission electron microscope (HRTEM). As an example, the Ag<sub>75</sub>Cu<sub>25</sub> particles are ranged from 1 nm to 3.5 nm and present many clearly lattice fringes on the surface. In **Figure 3b**, the inverse FFT of a particle exhibit that the surface of nanoparticles possess several difference lattice plane with d-spacing = 0.238 nm, 0.147 nm and 0.203 nm, which can be indexed to (111), (220) and (200) facets, respectively. As shown in **Figure 3c**, diffraction rings in selected area electron diffraction (SAED) also present the rings from (111), (220) and (200) faces, which is in agreement with the inverse FFT results. These results indicated the Ag<sub>75</sub>Cu<sub>25</sub> catalysts have various facets as the active surface. Previous research suggests that the catalytic reaction is not limited to (111) face but occurs also on (200)/(100), (220)/(110) and other faces.<sup>[7d, 17]</sup> These various active facets in Ag<sub>75</sub>Cu<sub>25</sub> alloys may result in a difference activity order with that calculated via DFT on (111) facet.<sup>16</sup> Meanwhile the surface composition and stability of as-prepared Ag-M catalysts were measured by XPS. As present in **Figure 3d** and **3e**, all samples exhibited a clear Ag peak and doping element (M) peaks which can be index to Ag<sup>0</sup> and M<sup>0</sup> metallic state (more details of XPS are shown in supporting information, see **Figure S8**).<sup>[18]</sup> These results suggest that the Ag-M alloys used in this work have a clean and well alloyed surface.

## 2.5. The long-term stability of the typical Ag<sub>75</sub>M<sub>25</sub> catalysts

Considering the low stability of Ag<sub>9</sub>Cu<sub>1</sub>/CNT as reported by Yi et al,<sup>[8]</sup> the long-term stability of Ag<sub>75</sub>Cu<sub>25</sub> alloys was measured in this work. The electrochemical durability of the Ag<sub>75</sub>Cu<sub>25</sub> catalyst was evaluated by using a line scan voltammetric accelerated stability test (LSV-AST) between 0.6 and 1.0 V (vs RHE) in O<sub>2</sub>-saturated 0.1 M KOH at a scan rate of 50

mV s<sup>-1</sup>. The ORR polarization curves of the Ag<sub>75</sub>Cu<sub>25</sub> catalyst after 9000 cycles are shown in **Figure 4a**. (details after each 1000 cycles were showed in supporting information, **Figure S9**). As present, after 9000 cycles, there was a slight decrease in half-wave potential for Ag<sub>75</sub>Cu<sub>25</sub> alloy from 0.76 V<sub>RHE</sub> to 0.75 V<sub>RHE</sub>. The ORR polarization curve after 9000 cycles present a peak at 0.3V<sub>RHE</sub>, indicating an obvious difference of the diffusion limiting current. Similar phenomena [6] has been reported in Ag-Co system that the Ag catalyst is sensitive to the electrolyte purity and the long term LSV-AST would influence the limit current of ORR polarization curve. **Figure 4b** and **Table S3** shows the the specific activity and ECSA of the Ag<sub>75</sub>Cu<sub>25</sub> catalyst investigated every 1000 cycles by Pb-stripping measurement, the ECSA decrease from 16.49 m<sup>2</sup> g<sub>total</sub><sup>-1</sup> to 14.24 m<sup>2</sup> g<sub>total</sub><sup>-1</sup> after LSV-AST cycles, the specific activity of Ag<sub>75</sub>Cu<sub>25</sub> alloy decreases from 0.851 mA cm<sup>-2</sup> to 0.834 mA cm<sup>-2</sup> during the LSV-AST cycles, its final specific activity was still as high as 0.834 mA cm<sup>-2</sup>, which is 2.8-fold higher than the initial value of pure Ag catalyst, suggesting that the Ag<sub>75</sub>Cu<sub>25</sub> catalyst has excellent long-term durability.

### 3. Conclusions

We have demonstrated that the relationships between specific activity and d-band center values in Ag<sub>75</sub>M<sub>25</sub> and Ag<sub>x</sub>Cu<sub>100-x</sub> alloys exhibit a volcano shape. From the volcano curve of Ag<sub>75</sub>M<sub>25</sub> alloys, we have established a new activity order for these alloys as Ag<sub>75</sub>Cu<sub>25</sub> > Ag<sub>75</sub>Fe<sub>25</sub> > Ag<sub>75</sub>Co<sub>25</sub> > Ag > Ag<sub>75</sub>In<sub>25</sub>. The activity study shows that the slight upshift in d-band center, approximately 0.12 eV, is beneficial for ORR activity in Ag<sub>75</sub>M<sub>25</sub> system. This result is in contrast to Pt-based alloys where the slight downshift (approximately 0.14 eV for Pt-Y) of d-band center improves ORR activity. For Ag<sub>75</sub>M<sub>25</sub> alloys, the Ag<sub>75</sub>Cu<sub>25</sub> exhibits the most activity with the best balance of the binding energy of oxygen and anions. We also studied the effect of copper content in the Ag<sub>x</sub>Cu<sub>100-x</sub> alloys and found a volcano curve for activity plot relative to Cu content. These results indicate that activity enhancement of Ag<sub>x</sub>Cu<sub>100-x</sub> alloys depend on the degree of alloying. Though Cu is suitable for modifying the

1 d-band center of Ag, excessive Cu on surface will block the active sites on  $\text{Ag}_x\text{Cu}_{100-x}$  surface  
2 and deteriorate the catalytic activity. Our results indicate that the  $\text{Ag}_{50}\text{Cu}_{50}$  alloy is most  
3  
4 active among  $\text{Ag}_x\text{Cu}_{100-x}$  alloys due to best balance between d-band position and the surface  
5  
6 Cu content. Moreover, the LSV-AST results confirm that the  $\text{Ag}_{75}\text{Cu}_{25}$  catalyst is stable in  
7  
8 alkaline solution even after 9000 cycles, indicating its excellent ORR stability. This work  
9  
10 suggests that it is feasible to increase the catalytic activity and stability of the Ag-based  
11  
12 nanoparticles by tuning the electronic properties, resulting in a new generation of Ag-Cu  
13  
14 systems with engineered alloying.  
15  
16  
17

## 18 **4. Materials and methods**

### 19 **4.1. Catalyst preparation.**

20  
21 We prepared polycrystalline nanoalloy catalysts of the type  $\text{Ag}_{75}\text{M}_{25}$  (M=Cu, Co, Fe and  
22  
23 In ) and  $\text{Ag}_x\text{Cu}_{100-x}$  (x=0, 25, 45, 50, 55, 75, 90 and 100) via the pulse laser deposition (PLD,  
24  
25 **Figure S1**) technology. This non-equilibrium vapor deposition technique ensures the  
26  
27 consistency of these alloys by exactly controlling target composition, evaporating temperature  
28  
29 and deposition time (details of this experiment have been shown in supporting  
30  
31 information).<sup>[19]</sup>  
32  
33  
34  
35  
36  
37

38  
39 The Ag-M alloys were in-situ deposited on glassy carbon electrode (GC,  $0.196\text{cm}^2$ ) via  
40  
41 PLD at  $1.0 \times 10^{-5}$  Pa atmospheric pressure. No binding materials (such as PTFE) and substrates  
42  
43 (such as carbon) were used between GC and Ag-M alloys. The GC was first cleaned in dilute  
44  
45 sulphuric acid for 5 mins, followed by washing in deionized water for 30 mins and drying in  
46  
47 vacuum oven (1 hours). The GC was then directly set on the side of adjustable rotation rate  
48  
49 sample platform (ARRSP) of the PLD. The  $\text{Ag}_{75}\text{M}_{25}$  (M=Fe, Co, Cu and In) and  $\text{Ag}_x\text{Cu}_{100-}$   
50  
51  $x$ (x=0, 25, 45, 50, 55, 75, 90, 100) sputtering targets were mounted on the side of adjustable  
52  
53 rotation rate target platform (ARRTP). Both the ARRSP and ARRTP rotated at the speed of 5  
54  
55 rpm and cooled by flowing Ar during the deposition process. The distance of the ARRSP - to  
56  
57 - ARRTP was 6 cm. To clean the surface of the targets, a nanosecond Q-switched Nd laser  
58  
59  
60  
61  
62  
63  
64  
65

1 irradiation (YAG laser beam with a wavelength of 266 nm and a pulse duration of 3-6 ns,  
2 beam diameter 1 mm with an energy density 200 mJ/pulse, EKSPLA, Lithuania) was  
3  
4 performed on the targets for 5 minutes at 2Hz. After this step, the Ag-M targets were allowed  
5  
6 to deposit onto the GC at 9 Hz. All of the catalyst samples were deposited with 4400 laser  
7  
8 pulses and the thickness and loading of Ag-M alloys on GC is  $12\mu\text{g cm}^{-2}$  as monitored by the  
9  
10 quartz crystal oscillation.  
11  
12

#### 13 **4.2. Catalyst characterisation.**

14  
15  
16 X-ray photoelectron spectroscopy (XPS) were measured on an ULTRA  
17  
18 (ESCALAB 250, Al  $K\alpha$ , ultrahigh vacuum is  $10^{-9}$ ,  $h\nu = 1486.6$  eV ). High-resolution  
19  
20 O1s, Cu2p and Ag3d spectra were acquired. No charge compensation was necessary.  
21  
22 The origin of the binding energy  $E_b$  was set to the Fermi energy  $E_f$  of the Au plate. The  
23  
24 Shirley background is subtracted from the measured spectra. The d-band center of the  
25  
26 valence band (VBS) is given by  $\int R(\epsilon)\epsilon d\epsilon / \int R(\epsilon) d\epsilon$ , where the  $R(\epsilon)$  is the XPS-intensity  
27  
28 after background subtraction.<sup>[14]</sup> The structure of the synthesized catalysts were  
29  
30 determined using an FEI Tecnai F30 transmission electron microscope (300 kV), a JEOL  
31  
32 JSM-6700F field-emission scanning electron microscope.  
33  
34  
35  
36  
37  
38

39 All electrochemical measurements were carried out by a classic three electrode set-up.  
40  
41 The Hg/HgO (0.1M) electrode was used as a reference electrode, a Pt wire electrode was  
42  
43 employed as a counter electrode. The working electrodes were fabricated by directly  
44  
45 depositing Ag-M alloys on GC. The catalyst loading was  $12\mu\text{g cm}^{-2}$ . Electrolyte solutions of  
46  
47 0.1 M KOH were prepared from ultrapure water ( $18.1\text{M}\Omega\text{ cm}^{-1}$ ) and 99.999% potassium  
48  
49 hydroxide. All solutions were freshly prepared before use and stored in a glove box to avoid  
50  
51 the contamination from the air (such as  $\text{CO}_2$ ). We considered IR-dropping in all of the tests.  
52  
53 All potentials are reported relative to the Reversible Hydrogen Electrode ( $V_{\text{RHE}} = V_{\text{NHE}} +$   
54  
55  $0.0591\text{pH}$ ).<sup>[6]</sup> The rotating disk electrode (RDE) and CHI660C electrochemical workstation  
56  
57 were performed to measure the electrocatalytic activity of the catalysts. The linear  
58  
59  
60  
61  
62  
63  
64  
65

1  
2  
3  
4  
5  
6  
7  
8  
9  
10  
11  
12  
13  
14  
15  
16  
17  
18  
19  
20  
21  
22  
23  
24  
25  
26  
27  
28  
29  
30  
31  
32  
33  
34  
35  
36  
37  
38  
39  
40  
41  
42  
43  
44  
45  
46  
47  
48  
49  
50  
51  
52  
53  
54  
55  
56  
57  
58  
59  
60  
61  
62  
63  
64  
65

voltammetry scanning (LSV) and rotating disk electrode (RDE) polarization curves were studied at room temperature in 0.1 M KOH(O<sub>2</sub> saturated). The scanning rate of these experiments were set as 10 mV s<sup>-1</sup> and the rotation rates were controlled at 400, 900, 1600 and 2500 rpm.

Pb-stripping voltammetry was performed immediately after ORR measurements in 0.1M KOH+125μM Pb(NO<sub>3</sub>)<sub>2</sub> solution. Before Pb-stripping voltammetry test, the solution was purged with Ar for 30 minutes. The initial potential were set at 0.2V<sub>RHE</sub> and the final potential is 0.6 V<sub>RHE</sub>. The stable voltammograms were integrated assuming 280uC/cm<sup>2</sup>, which was established based on Ag faces.<sup>[20]</sup>

### Supporting Information

Supporting Information is available from the Wiley Online Library or from the author.

### Acknowledgments

This study was supported by the National Natural Science Foundation of China (grant nos. 51271148 and 50971100), the Research Fund of State Key Laboratory of Solidification Processing in China (grant no. 150-ZH-2016), the Aeronautic Science Foundation Program of China (grant no. 2012ZF53073), the Science and Technology Innovation Fund of Western Metal Materials (grant no. XBCL-2-11) and the Doctoral Fund of Ministry of Education of China (grant no. 20136102110013).

## References

1. a) L.Q. Mao; D. Zhang; T. Sotomura; K. Nakatsu; N. Koshiba; T. Ohsaka, *Electrochim. Acta* **2003**, *48*, 1015-1021; b) D.L. Wang; H.L. Xin; Y.C. Yu; H.S. Wang; E. Rus; D.A. Muller; H.D. Abruna, *J. Am. Chem. Soc.* **2010**, *132*, 17664-17666.
2. a) M. Chatenet; L. Genies-Bultel; M. Aurousseau; R. Durand; F. Andolfatto, *Appl. Electrochem.* **2002**, *32*, 1131-1140; b) Y. Li; H. Dai, *Chem. Soc. Rev.* **2014**, *43*, 5257-75; c) A. Qaseem; F. Chen; X. Wu; R.L. Johnston, *Catal. Sci. Technol.* **2016**.
3. a) T. Hofmann; T.H. Yu; M. Folsie; L. Weinhardt; M. Bär; Y. Zhang; B.V. Merinov; D.J. Myers; W.A. Goddard; C. Heske, *J. Phys. Chem. C* **2012**, *116*, 24016-24026; b) K. Shin; D.H. Kim; S.C. Yeo; H.M. Lee, *Catal. Today* **2012**, *185*, 94-98; c) N. Wagner; M. Schulze; E. Gülzow, *J. Power Sources* **2004**, *127*, 264-272; d) J.L. Fernandez; D.A. Walsh; A.J. Bard, *J. Am. Chem. Soc.* **2005**, *127*, 357-365; e) F.H.B. Lima; J.F.R. de Castro; E.A. Ticianelli, *J. Power Sources* **2006**, *161*, 806-812.
4. a) X.Q. Wu; F.Y. Chen; N. Zhang; A. Qaseem; R.L. Johnston, *J. Mater. Chem. A* **2016**, *4*, 3527-3537; b) X.Q. Wu; F.Y. Chen; Y.C. Jin; N. Zhang; R.L. Johnston, *ACS Appl. Mater. Interfaces* **2015**, *7*, 17782-17791.
5. a) S. Jong Yoo; S.K. Kim; T.Y. Jeon; S. Jun Hwang; J.G. Lee; S.C. Lee; K.S. Lee; Y.H. Cho; Y.E. Sung; T.H. Lim, *Chem. Commun.* **2011**, *47*, 11414-6; b) Y.T. Liang; S.P. Lin; C.W. Liu; S.R. Chung; T.Y. Chen; J.H. Wang; K.W. Wang, *Chem. Commun.* **2015**, *51*, 6605-6608; c) V. Stamenkovic; B.S. Mun; K.J.J. Mayrhofer; P.N. Ross; N.M. Markovic; J. Rossmeisl; J. Greeley; J.K. Nørskov, *Angew. Chem.* **2006**, *118*, 2963-2967.
6. A. Holewinski; J.C. Idrobo; S. Linic, *Nat. Chem.* **2014**, *6*, 828-34.
7. a) B. Lim; M.J. Jiang; P.H.C. Camargo; E.C. Cho; J. Tao; X.M. Lu; Y.M. Zhu; Y.N. Xia, *Science* **2009**, *324*, 1302-1305; b) D.Y. Wang; H.L. Chou; C.C. Cheng; Y.H. Wu; C.M. Tsai; H.Y. Lin; Y.L. Wang; B.J. Hwang; C.C. Chen, *Nano Energy* **2015**, *11*, 631-639; c) Q.Y. Wang; X.Q. Cui; W.M. Guan; L. Zhang; X.F. Fan; Z. Shi; W.T. Zheng, *J. Power Sources* **2014**, *269*, 152-157; d) L. Bu; J. Ding; S. Guo; X. Zhang; D. Su; X. Zhu; J. Yao; J. Guo; G. Lu; X. Huang, *Adv. Mater.* **2015**, *27*, 7204-12.
8. Q.F. Yi; H. Chu; M.X. Tang; Z. Yang; Q.H. Chen; X.P. Liu, *J. Electroanal. Chem.* **2015**, *739*, 178-186.
9. K. Shin; H. Kim da; H.M. Lee, *ChemSusChem* **2013**, *6*, 1044-9.
10. N. Zhang; F.Y. Chen; X.Q. Wu, *Sci. Rep.* **2015**, *5*.
11. a) Y.C. Jin; F.Y. Chen; Y.M. Lei; X.Q. Wu, *Chemcatchem* **2015**, *7*, 2377-2383; b) Y.C. Jin; F.Y. Chen, *Electrochim. Acta* **2015**, *158*, 437-445.
12. X.Z. Li; Y.Y. Fang; X.Q. Lin; M. Tian; X.C. An; Y. Fu; R. Li; J. Jin; J.T. Ma, *J. Mater. Chem. A* **2015**, *3*, 17392-17402.
13. a) J. Masa; C. Batchelor-McAuley; W. Schuhmann; R.G. Compton, *Nano Res.* **2014**, *7*, 71-78; b) Y. Lu; Y. Wang; W. Chen, *J. Power Sources* **2011**, *196*, 3033-3038; c) R.R. Chen; H.X. Li; D. Chu; G.F. Wang, *J. Phys. Chem. C* **2009**, *113*, 20689-20697.
14. S.J. Hwang; S.K. Kim; J.G. Lee; S.C. Lee; J.H. Jang; P. Kim; T.H. Lim; Y.E. Sung; S.J. Yoo, *J. Am. Chem. Soc.* **2012**, *134*, 19508-11.
15. V.R. Stamenkovic; B.S. Mun; M. Arenz; K.J. Mayrhofer; C.A. Lucas; G. Wang; P.N. Ross; N.M. Markovic, *Nat. Mater.* **2007**, *6*, 241-7.
16. V. Stamenkovic; B.S. Mun; K.J.J. Mayrhofer; P.N. Ross; N.M. Markovic; J. Rossmeisl; J. Greeley; J.K. Nørskov, *Angew. Chem. Int. Ed.* **2006**, *45*, 2897-2901.
17. a) Y. Zhou; Q. Lu; Z.B. Zhuang; G.S. Hutchings; S. Kattel; Y.S. Yan; J.G.G. Chen; J.Q. Xiao; F. Jiao, *Adv. Energy Mater.* **2015**, *5*; b) V.R. Stamenkovic; B. Fowler; B.S. Mun; G. Wang; P.N. Ross; C.A. Lucas; N.M. Markovic, *Science* **2007**, *315*, 493-7.
18. F.M. John; F.S. William; E.S. Peter; D.B. Kenneth, *Handbook of X-ray Photoelectron Spectroscopy*. Perkin-Elmer Corporation Physical Electronics Division: Eden Prairie: Unite states of America, 1992; p 261.
19. S.J. Chung; A. Roy; D.H. Hong; J.P. Leonard; P.N. Kumta, *Mater. Sci. Eng. B* **2011**, *176*, 1690-1694.
20. E. Kirowa-Eisner; D. Tzur; E. Gileadi, *J. Electroanal. Chem.* **2008**, *621*, 146-158.

**Table 1.** The ORR activity parameters: half-wave potential ( $E_{half}$ ), kinetic currents ( $j_{kc}$ ), mass-corrected kinetic current ( $j_{mass}$ ), electrochemical surface areas (ECSA,  $m^2 g_{total}^{-1}$ ) and Tafel slopes ( $mV dec^{-1}$ ) of the  $Ag_{75}M_{25}$  and  $Ag_xCu_{100-x}$  catalysts in  $O_2$ -saturated 0.1 M KOH in positive direction at scan rate of  $10 mVs^{-1}$  and with electrode rotation frequency of 1600 rpm.

Catalyst	Half-	Mass-corrected							
	wave	Current density				kinetic current	ECSA	Tafel plots	
	potential	(mA cm <sup>-2</sup> )				at 0.85V <sub>RHE</sub>	(m <sup>2</sup> g <sub>total</sub> <sup>-1</sup> )	(mV dec <sup>-1</sup> )	
	(V <sub>RHE</sub> )					(A g <sub>total</sub> <sup>-1</sup> )		Low	High
		$E_{half}$	$j$	$j_d$	$j_{kc}$	$j_{mass}$	A	overpotentials	overpotentials
Ag	0.66	0.3	4.12	0.32	26.7	14.05	79	138	
$Ag_{75}In_{25}$	0.56	0.01	4.20	0.01	0.8	15.22	81	147	
$Ag_{75}M_{25}$ $Ag_{75}Co_{25}$	0.70	0.64	4.14	0.76	63.3	15.79	78	131	
$Ag_{75}Fe_{25}$	0.73	0.75	4.15	0.92	76.7	15.65	76	129	
$Ag_{75}Cu_{25}$	0.76	0.85	4.19	1.07	89.5	16.49	72	108	
$Ag_{90}Cu_{10}$	0.69	0.47	4.16	0.53	44.2	15.56	78	110	
$Ag_{55}Cu_{45}$	0.81	1.28	4.21	1.85	154.2	15.93	69	106	
$Ag_xCu_{100-x}$ $Ag_{50}Cu_{50}$	0.82	1.57	4.21	2.49	207.5	16.90	64	104	
$Ag_{45}Cu_{55}$	0.81	1.49	4.15	2.33	194.2	16.43	59	106	
$Ag_{25}Cu_{75}$	0.71	0.55	4.13	0.63	52.5	15.93	75	112	
Pt/C-20%	0.88	1.72	4.23	2.90	241.6	--	58	64	

$j$  of  $Ag_{75}M_{25}$  and  $Ag_xCu_{100-x}$  catalysts is the total current density at 0.85 V<sub>RHE</sub>,  $j$  of Pt/C-20% is the total current density at 0.90 V<sub>RHE</sub>.

$j_d$  is the diffusion limited current density

$j_{kc}$  is the kinetic current at 0.85V<sub>RHE</sub>.

$j_{mass}$  is the mass-corrected kinetic current at 0.85V<sub>RHE</sub>.



**Table 2.** The position of d-band centre and specific activity (SA) of the Ag<sub>75</sub>M<sub>25</sub> and Ag<sub>x</sub>Cu<sub>100-x</sub> catalysts

Catalyst	Position of d-band center, $E_d$ (eV)	Up-shift d-band Center, $\Delta E_d$ (eV)	SA at 0.85V <sub>RHE</sub> $J_s$ (mA cm <sup>-2</sup> )	Improvement of SA $\Delta J_s$ (mA cm <sup>-2</sup> )
Ag	-5.28	0	0.3	0
Ag <sub>75</sub> In <sub>25</sub>	-5.51	-0.23	0.01	-0.29
Ag <sub>75</sub> M <sub>25</sub> Ag <sub>75</sub> Co <sub>25</sub>	-4.45	0.83	0.64	0.34
Ag <sub>75</sub> Fe <sub>25</sub>	-4.71	0.57	0.75	0.45
Ag <sub>75</sub> Cu <sub>25</sub>	-5.16	0.12	0.95	0.65
Ag <sub>90</sub> Cu <sub>10</sub>	-5.21	0.07	0.47	0.17
Ag <sub>55</sub> Cu <sub>45</sub>	-4.98	0.30	1.28	0.98
Ag <sub>x</sub> Cu <sub>100-x</sub> Ag <sub>50</sub> Cu <sub>50</sub>	-4.92	0.36	1.57	1.27
Ag <sub>45</sub> Cu <sub>55</sub>	-4.8	0.48	1.49	1.19
Ag <sub>25</sub> Cu <sub>75</sub>	-4.7	0.58	0.55	0.25

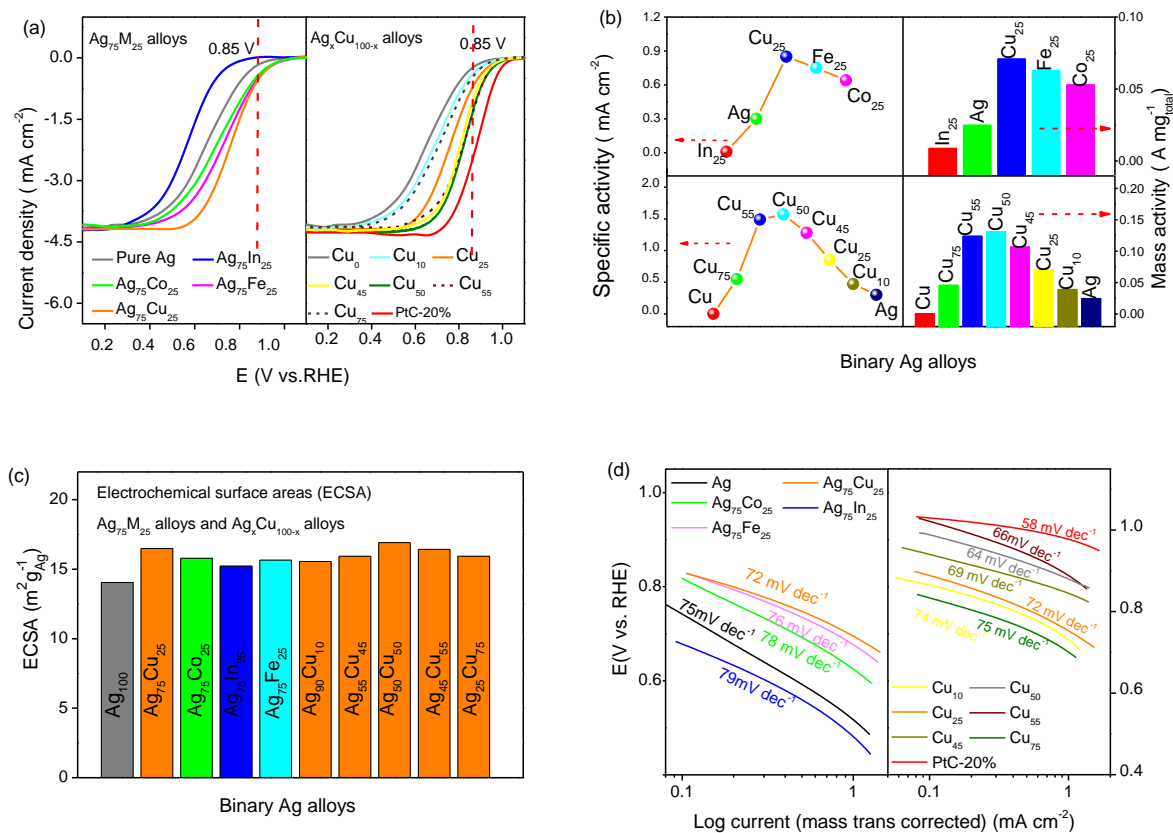


**Figure 1.** (a) The ORR polarization curves of Ag<sub>75</sub>M<sub>25</sub> (M: Cu, Co, Fe and In) alloys, Ag<sub>x</sub>Cu<sub>100-x</sub> (x= 0, 25, 45, 50, 55, 75, 90 and 100) alloys ; Electrolyte: O<sub>2</sub> saturated 0.1M KOH solution, room temperature; sweep rate, 10 mV s<sup>-1</sup>; rotation rate, 1600 rpm; loading of Ag<sub>75</sub>M<sub>25</sub> and Ag<sub>x</sub>Cu<sub>100-x</sub> : 12 μg cm<sup>-2</sup>. (b) Relationships between experimentally measured specific activity (SA) and mass activity (MA) of Ag<sub>75</sub>M<sub>25</sub>, and Ag<sub>x</sub>Cu<sub>100-x</sub> alloys at 0.85V<sub>RHE</sub> versus the compositions of M. (c) The corresponding electrochemical surface areas (ECSA) of Ag<sub>75</sub>M<sub>25</sub> and Ag<sub>x</sub>Cu<sub>100-x</sub> alloys. (d) The mass-transport corrected kinetic current Tafel plots for the Ag<sub>75</sub>M<sub>25</sub> and Ag<sub>x</sub>Cu<sub>100-x</sub> alloys.

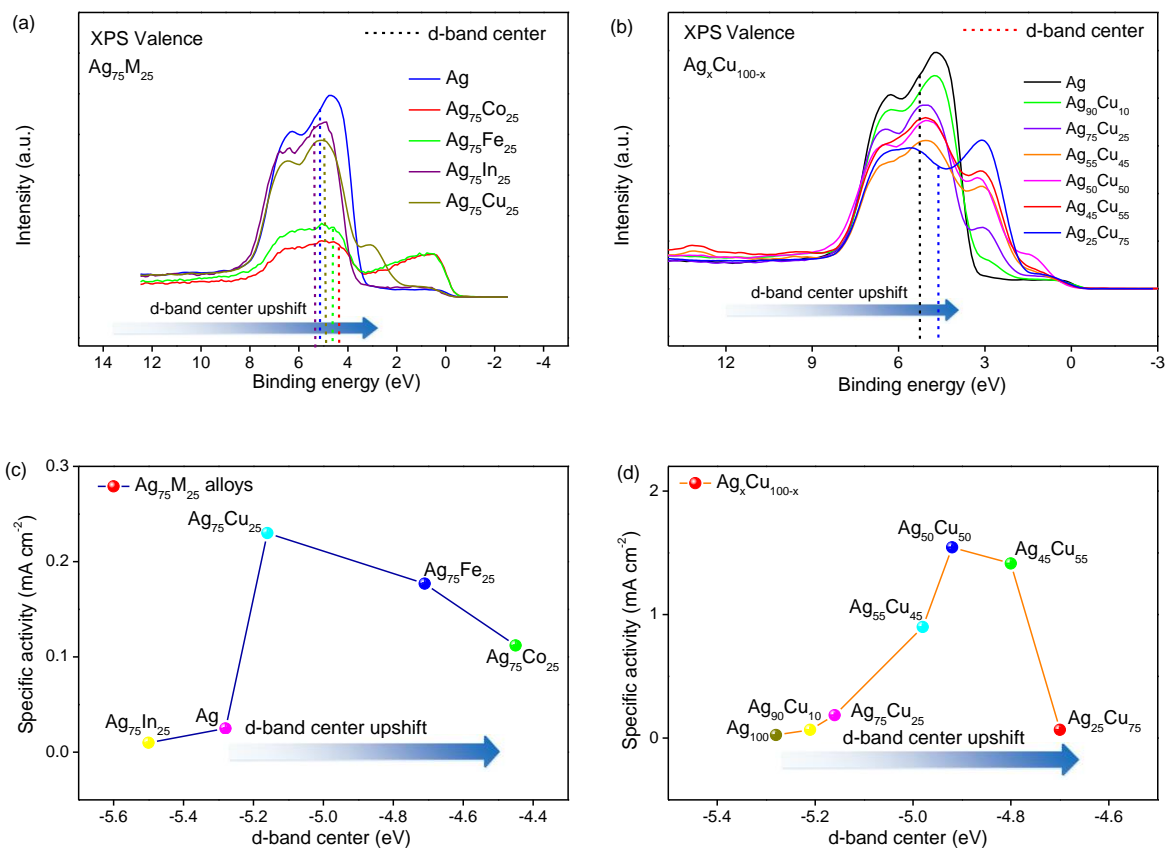


**Figure 2.** Valence band spectra (VBS) of (a) the  $\text{Ag}_{75}\text{M}_{25}$  and (b)  $\text{Ag}_x\text{Cu}_{100-x}$  alloys as measured by high-resolution X-ray photoelectron spectroscopy. (c) Relationships between experimentally measured specific activity (SA) at  $0.85\text{V}_{\text{RHE}}$  versus the d-band center position for  $\text{Ag}_{75}\text{M}_{25}$  alloys with various kinds of alloy composition. (d) Relationships between specific activity (SA) at  $0.85\text{V}_{\text{RHE}}$  versus the d-band center position for  $\text{Ag}_x\text{Cu}_{100-x}$  alloys with various content of Cu.

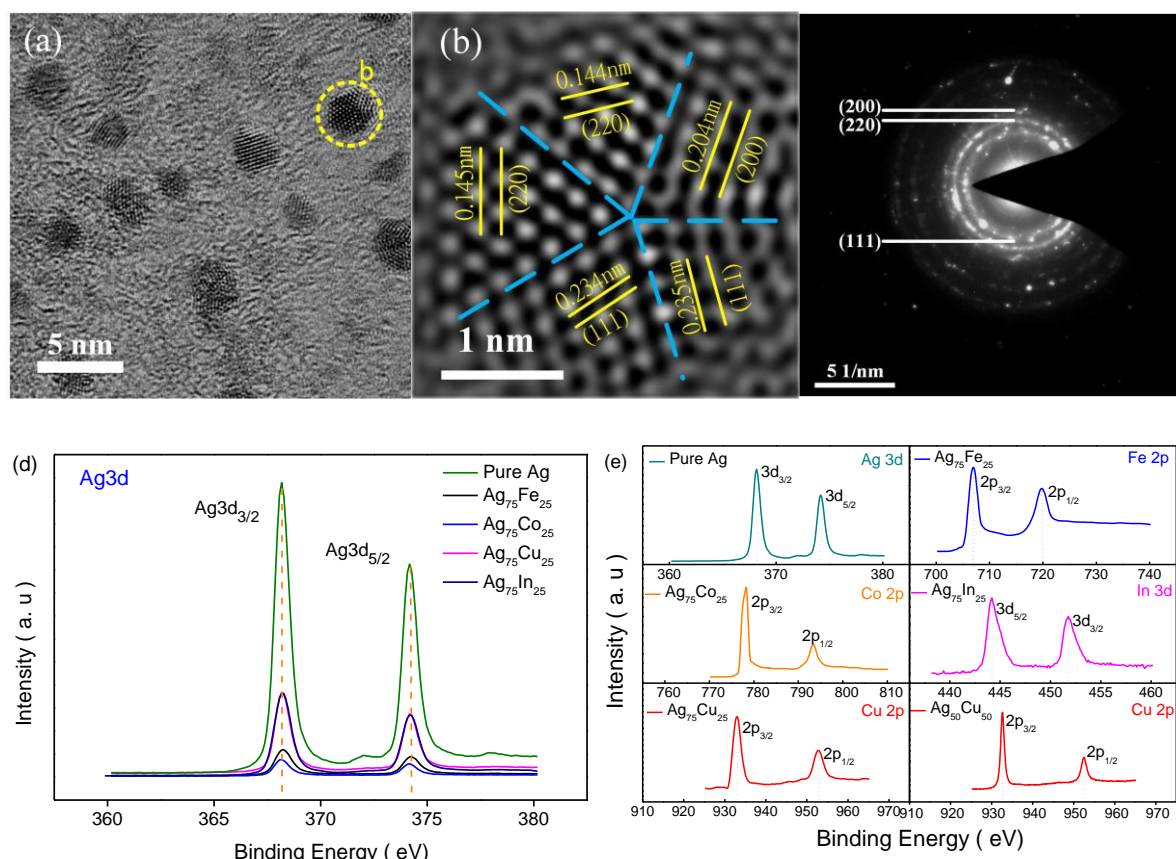


**Figure 3.** (a) Typical HRTEM images of the Ag-M ( $\text{Ag}_{75}\text{Cu}_{25}$ ) alloy, (b) the inverse FFT for the particle b, (c) typical selected area electron diffraction (SAED) of the Ag-M alloy ( $\text{Ag}_{75}\text{Cu}_{25}$ ) alloy, (d) XPS of Ag3d regions for pure Ag,  $\text{Ag}_{75}\text{Fe}_{25}$ ,  $\text{Ag}_{75}\text{In}_{25}$ ,  $\text{Ag}_{75}\text{Co}_{25}$  and  $\text{Ag}_{75}\text{Cu}_{25}$  alloys, (e) XPS of Ag 3d, Fe 2p, Co 2p, Cu 2p and In 3d regions for Pure Ag,  $\text{Ag}_{75}\text{Fe}_{25}$ ,  $\text{Ag}_{75}\text{Co}_{25}$ ,  $\text{Ag}_{75}\text{In}_{25}$ ,  $\text{Ag}_{75}\text{Cu}_{25}$  and  $\text{Ag}_{50}\text{Cu}_{50}$  alloys.

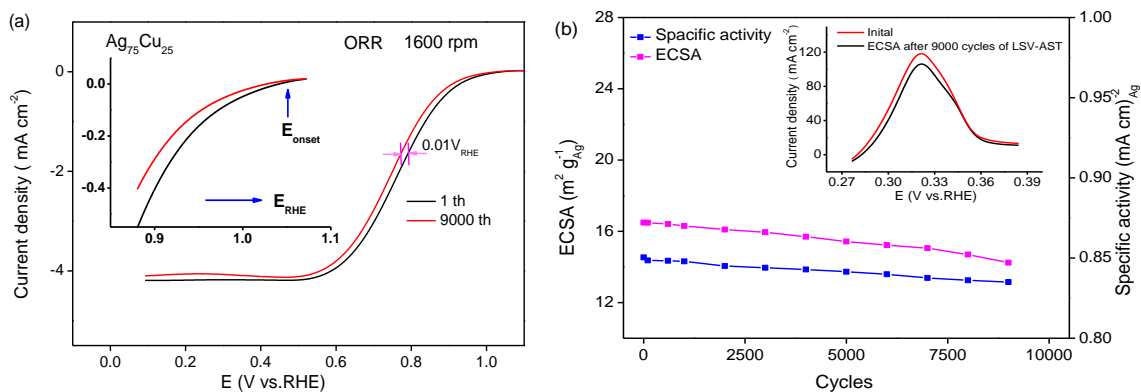


**Figure 4.** (a) A comparison of ORR polarization curves before and after 9000 cycles of line scan voltammetric accelerated stability tests (LSV-AST) for the  $\text{Ag}_{75}\text{Cu}_{25}$  catalysts in  $\text{O}_2$ -saturated 0.1 M KOH; sweep rate was  $10 \text{ mVs}^{-1}$  and rotating rate was 1600 rpm. (b) The corresponding electrochemical surface areas (ECSA) and specific activity (SA) of  $\text{Ag}_{75}\text{Cu}_{25}$  catalysts on each stage of LSV-AST.

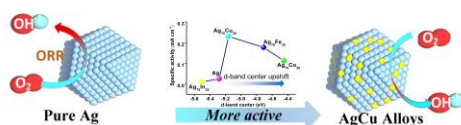
The ORR activity trends of binary silver alloy nanocatalysts were discussed, which is highly dependence on the d-band center of valence band spectrum. The results present that the up shift d-band center is benefit for ORR and the optimal  $\text{Ag}_{50}\text{Cu}_{50}$  catalyst (0.1eV) shows highly activity and durability for ORR in alkaline media, which is comparable to the commercial Pt/C-20% catalyst.

**Keyword: binary silver alloy, activity trends, d-band center, valence band spectrum**

Xiaoqiang Wu,<sup>[a]</sup> Fuyi Chen,<sup>\*[a]</sup> Nan Zhang,<sup>[a]</sup> Yimin Lei,<sup>[a]</sup> Yachao Jin,<sup>[a]</sup> Adnan Qaseem,<sup>[a]</sup> and Roy L. Johnston<sup>[b]</sup>

### Activity Trends of Binary Silver Alloy Nanocatalysts for Oxygen Reduction Reaction in Alkaline Media

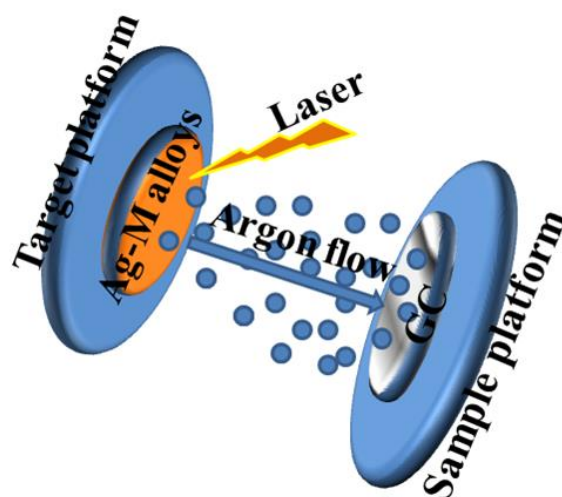
#### TOC:



## Supporting Information

### Activity Trends of Binary Silver Alloy Nanocatalysts for Oxygen Reduction Reaction in Alkaline Media

*Xiaoqiang Wu,<sup>[a]</sup> Fuyi Chen,<sup>\*,[a]</sup> Nan Zhang,<sup>[a]</sup> Yimin Lei,<sup>[a]</sup> Yachao Jin,<sup>[a]</sup> Adnan Qaseem,<sup>[a]</sup> and Roy L. Johnston<sup>[b]</sup>*

*Part 1. Preparation of the Ag-M alloys.*1  
2  
3  
4  
5  
6  
7  
8  
9  
10  
11  
12  
13  
14  
15  
16  
17  
18  
19  
20  
21  
22  
23  
24  
25  
26  
27  
28  
29  
30  
31  
32  
33  
34  
35  
36  
37  
38  
39  
40  
41  
42  
43  
44  
45  
46  
47  
48  
49  
50  
51  
52  
53  
54  
55  
56  
57  
58  
59  
60  
61  
62  
63  
64  
65**Figure S1.** Preparation of Ag-M electrodes.

To ensure the accuracy of the experimental results, the Ag-M alloys were in-situ deposited on glassy carbon electrode (GC,  $0.196\text{cm}^2$ ) via pulse laser deposition (PLD) at  $1.0 \times 10^{-5}$  Pa atmospheric pressure. No binding materials (such as PTFE) and substrates (such as carbon) were used between GC and Ag-M alloys. The GC was first cleaned in dilute sulphuric acid for 5 mins, followed by washing in deionized water for 30 mins and drying in vacuum oven (1 hours). The GC was then directly set on the side of adjustable rotation rate sample platform (ARRSP) of the PLD. The  $\text{Ag}_{75}\text{M}_{25}$  ( $\text{M}=\text{Fe}$ ,  $\text{Co}$ ,  $\text{Cu}$  and  $\text{In}$ ) and  $\text{Ag}_x\text{Cu}_{100-x}$  ( $x=0, 25, 45, 50, 55, 75, 90, 100$ ) sputtering targets were fixed on the side of adjustable rotation rate target platform (ARRTP). Both the ARRSP and ARRTP rotated at the speed of 5 rpm and cooled by flowing Ar during the deposition process. The distance of the ARRSP - to - ARRTP was 6cm. To clean the surface of the targets, nanosecond Q-switched Nd laser irradiation (YAG laser beam with a wavelength of 266 nm and a pulse duration of 3-6 ns, beam diameter 1 mm with an energy density 200 mJ/pulse, EKSPLA, Lithuania) was performed on the targets for 5 minutes at 2Hz. After this process, the Ag-M targets were allowed to deposit onto the GC at 9 Hz. All of the catalyst samples were deposited with 4400 laser pulses (The loading of Ag-M alloys on GC is  $12\mu\text{g cm}^{-2}$ ).



## Part 2. Electrochemical measurements

### Oxygen reduction reaction tests (ORR)

All electrochemical measurements were carried out by a classic three electrode set-up. The Hg/HgO (0.1M) electrode was used as a reference electrode, a Pt wire electrode was employed as a counter electrode. The working electrodes were fabricated by directly depositing Ag-M alloys on GC. The catalyst loading was  $12 \mu\text{g cm}^{-2}$ . Electrolyte solutions of 0.1 M KOH were prepared from ultrapure water ( $18.1\text{M}\Omega \text{ cm}^{-1}$ ) and 99.999% potassium hydroxide. All solutions were freshly prepared before use and stored in a glove box to avoid the contamination from the air (such as  $\text{CO}_2$ ). We considered IR-dropping in all of the tests. All potentials are reported relative to the Reversible Hydrogen Electrode ( $V_{\text{RHE}} = V_{\text{NHE}} + 0.0591\text{pH}$ ).<sup>[1]</sup> The rotating disk electrode (RDE) and CHI660C electrochemical workstation were performed to measure the electrocatalytic activity of the catalysts. The linear voltammetry scanning (LSV) and rotating disk electrode (RDE) polarization curves were studied at room temperature in 0.1 M KOH ( $\text{O}_2$  saturated). The scanning rate of these experiments were set as  $10 \text{ mV s}^{-1}$  and the rotation rates were controlled at 400, 900, 1600 and 2500 rpm.

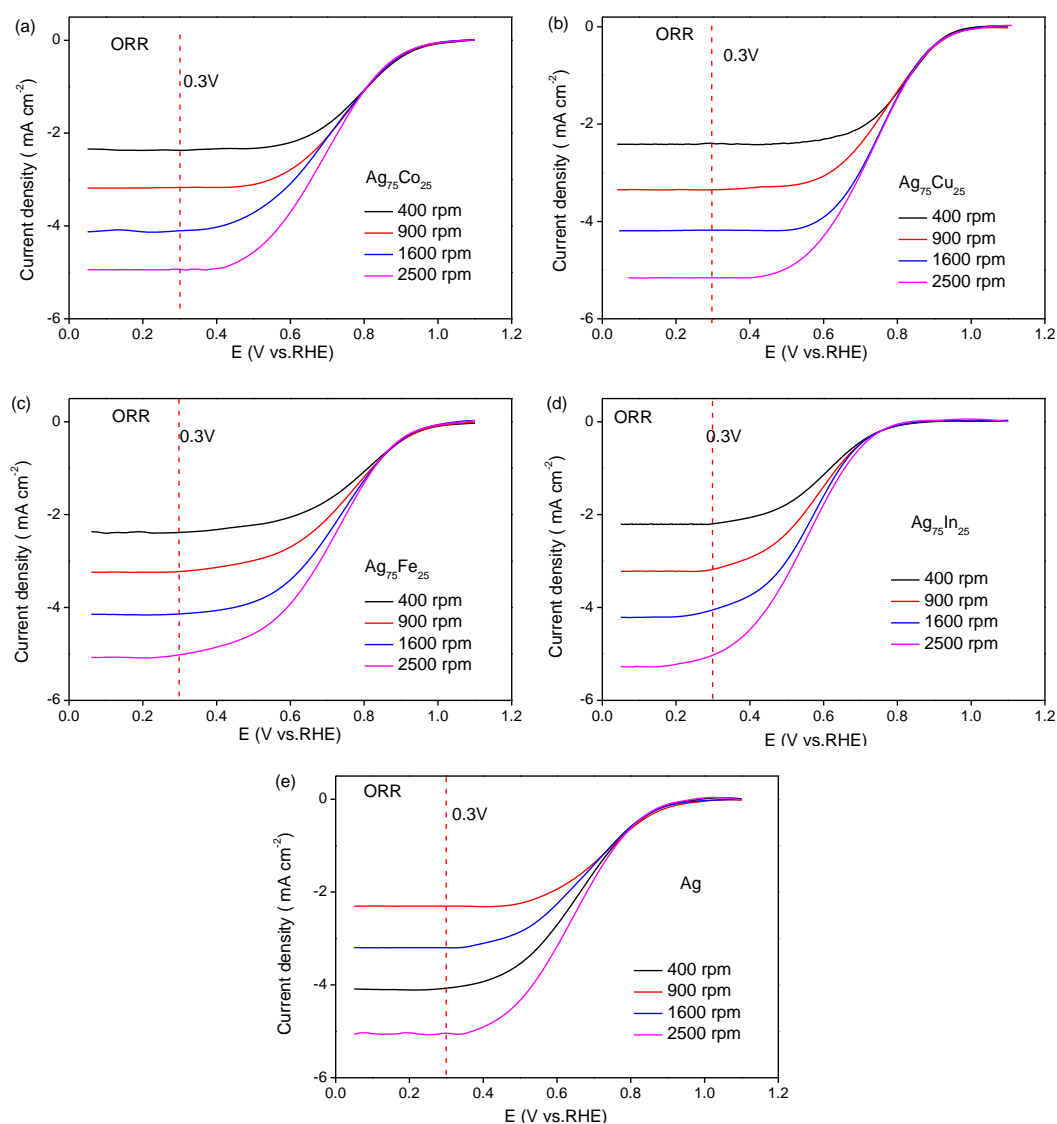


**Figure S2.** The ORR polarization curves of  $\text{Ag}_{75}\text{M}_{25}$  alloys.

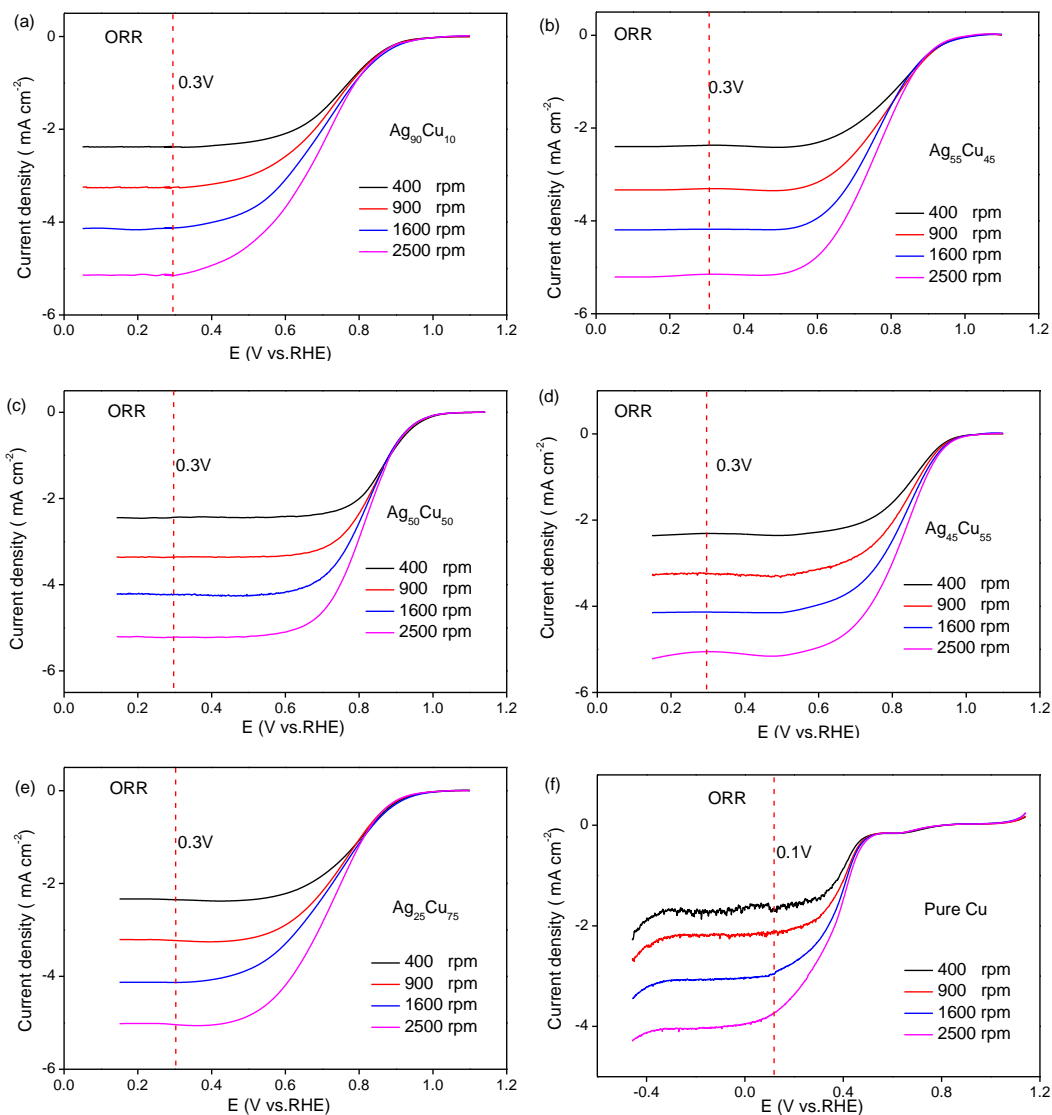


**Figure S3.** The ORR polarization curves of  $\text{Ag}_x\text{Cu}_{100-x}$  alloys.

### Koutecky-Levich (KL) analysis and Tafel plots

The Koutecky-Levich equation was applied to calculate kinetic current density based on ORR polarization curve. The number ( $n$ ) of electrons transferred in the ORR process can be obtained from the slope of the Koutecky-Levich plot.<sup>[2]</sup>

$$j^{-1} = j_k^{-1} + (0.62nFCD^{2/3}v^{-1/6}\omega^{1/2})^{-1} \quad (1)$$

Where  $j$  is the measured electrode current density,  $j_k$  is the kinetic current density, and  $\omega$  is the electrode rotation rate. The value of  $D$  is  $1.9 \times 10^{-5} \text{ cm}^2/\text{s}$ ,  $C_0$  is  $1.2 \times 10^{-6} \text{ mol}/\text{cm}^3$ ,  $v$  is  $1.1 \times 10^{-2} \text{ cm}^2/\text{s}$ , and  $F$  is  $96485 \text{ C}/\text{mol}$ .

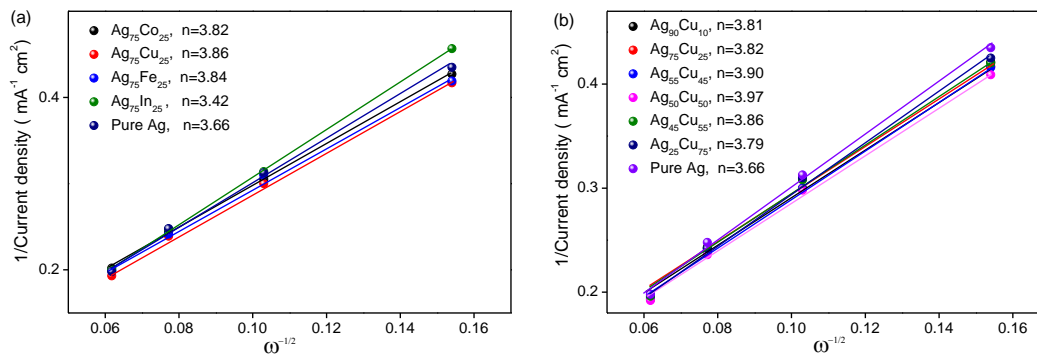


**Figure S4.** Koutecky-Levich plots collected from corresponding RDE polarization curves of Ag-M alloys at  $0.3V_{\text{RHE}}$ .

### Tafel plots analysis

The catalyst film on GC was made thin and smooth via PLD, so that its effect on the kinetic parameters was negligible. Tafel plots were constructed from the corresponding polarization curves, in which the kinetic current densities were calculated by mass-transport correction as follows:<sup>[3]</sup>

$$J_{\text{kc}} = (J_i \times J) \times (J_i - J)^{-1} \quad (2)$$

where  $J_i$  is the diffusion limited current density and  $J$  is the real current density as measured in ORR polarization curves.

### Electrochemically active surface area (ECSA) analysis

Pb-stripping voltammetry was performed immediately after ORR measurements in 0.1M KOH+125 $\mu$ M Pb(NO<sub>3</sub>)<sub>2</sub> solution. Before Pb-stripping voltammetry test, the solution was purged with Ar for 30 minutes. The initial potential were set at 0.2V<sub>RHE</sub> and the final potential is 0.6 V<sub>RHE</sub>. The stable voltammograms were integrated assuming 280 $\mu$ C/cm<sup>2</sup>, which was established based on Ag faces.<sup>[4]</sup> The ECSA were calculated by equation as follow:

$$\text{ECSA} = Q_h / 280 \quad (3)$$

Where the  $Q_h$  is surface charge that can be calculated from the area under the CV by equation as follow:

$$Q_h = \int j(E) dE \times (V \times m)^{-1} \quad (3)$$

Where the  $j(E)$  is the real current density as shown in Figure S5,  $V$  is the scan rate. In this work, the scan rate is 10mV/s.

**Table S1.** Comparisons of Pb-stripping area, surface charge and ECSA of Ag<sub>75</sub>M<sub>25</sub> and Ag<sub>x</sub>Cu<sub>100-x</sub> catalysts.

Catalyst	Area of Pb-stripping (A)	Surface charge (Q <sub>h</sub> )	ECSA	Change of ECSA relative to pure Ag $\Delta$ ECSA
	$\int j(E)dE$	$\times 10^6 \mu\text{C}$	$\text{m}^2/\text{g}_{\text{Ag}}$	$\text{m}^2/\text{g}_{\text{Ag}}$
Ag	472.1	39.33	14.05	0
Ag <sub>75</sub> M <sub>25</sub>	Ag <sub>75</sub> In <sub>25</sub>	511.4	42.62	1.17
	Ag <sub>75</sub> Co <sub>25</sub>	530.5	44.21	1.74
	Ag <sub>75</sub> Fe <sub>25</sub>	525.9	43.83	1.60
	Ag <sub>75</sub> Cu <sub>25</sub>	554.0	46.16	16.49
Ag <sub>x</sub> Cu <sub>100-x</sub>	Ag <sub>90</sub> Cu <sub>10</sub>	521.3	43.45	1.51
	Ag <sub>55</sub> Cu <sub>45</sub>	535.4	44.61	15.93
	Ag <sub>50</sub> Cu <sub>50</sub>	568.4	47.33	16.90
	Ag <sub>45</sub> Cu <sub>55</sub>	552.2	46.02	16.43
	Ag <sub>25</sub> Cu <sub>75</sub>	535.4	44.61	15.93

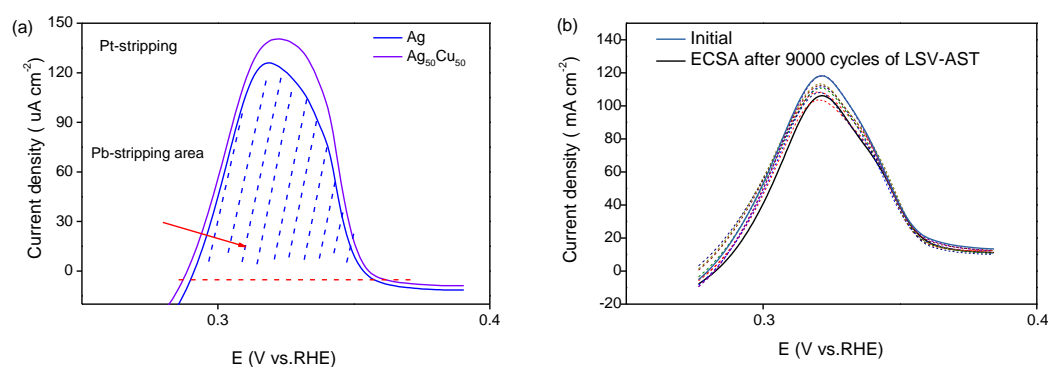


**Figure S5.** (a) the corresponding electrochemical surface areas (ECSA) of Ag-M alloys. (b) the corresponding ECSA of Ag<sub>75</sub>Cu<sub>25</sub> alloy after 100, 600, 1000, 2000, 3000, 4000, 5000, 6000, 7000, 8000 and 9000 cycles accelerated stability test.

### Part 3. The model and calculation methods.

The DFT calculations are carried out by using the Dmol3 package. The exchange-correlation potential is treated with the GGA-PBE functional. The orbital cutoff range was set to 5.0 Å and the Fermi smearing was set to  $1.0 \times 10^{-5}$  Ha. The DFT semi-core pseudo potential was used to treat the core electrons of heavy Ag and Cu atoms. The convergence tolerances of energies, forces and displacements were  $1.0 \times 10^{-5}$  Ha, 0.002 Ha/Å and 0.005 Å, respectively. We used a periodic slab to model the clean and Cu-decorated Ag(111) surfaces, which were repeated in a  $(2 \times 2)$  surface unit cell while having four atomic layers and a vacuum gap of 14 Å in the z-direction.

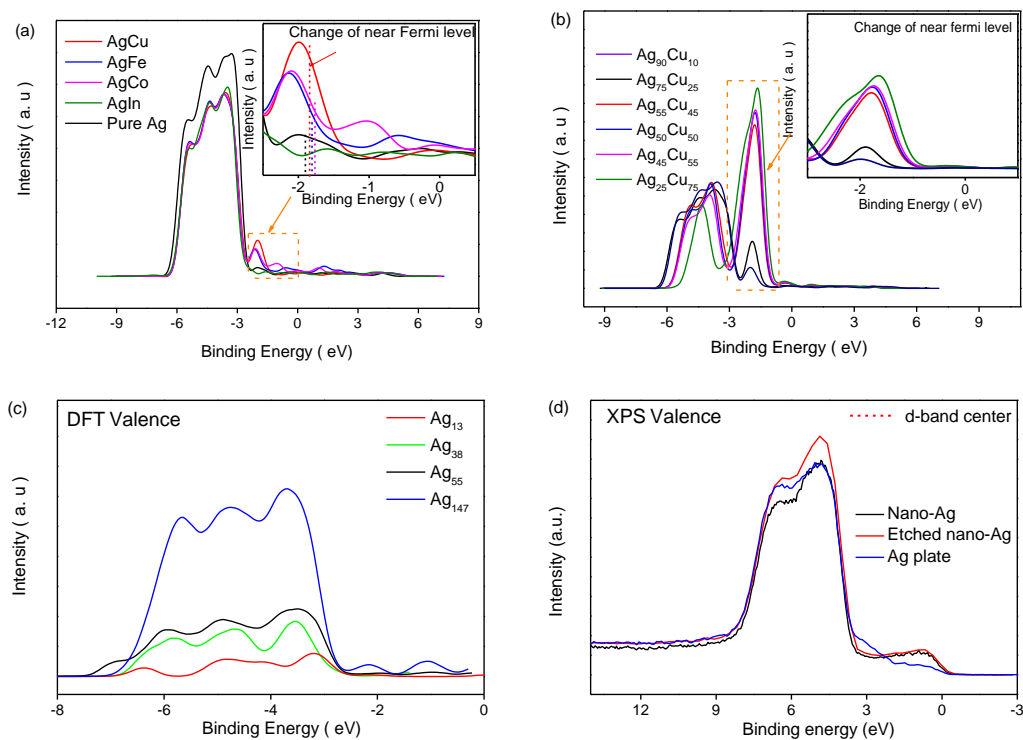


**Figure S6.** (a) Valence band spectra (VBS) of (a) Ag<sub>75</sub>M<sub>25</sub> alloys calculate by density function theory(DTF). (b) Valence band spectra (VBS) of (a) Ag<sub>x</sub>Cu<sub>100-x</sub> alloys calculate by density function theory(DTF). (c) VBS of Ag<sub>13</sub>,Ag<sub>38</sub>,Ag<sub>55</sub> and Ag<sub>147</sub> measured by DFT.(d) The VBS of nano-Ag, etched nano-Ag and Ag plate measured by XPS.

Table S2. Comparison of the position of d-band centre and change of DOS(near fermi level)

Catalyst	Position of d-band center $E_d$ (eV)	Up-shift d-band center $\Delta E_d$ (eV)	Intensity of DOS (between 0eV to -3eV ) $\int R(\epsilon)d\epsilon$	Change of DOS (between 0eV to -3eV ) $\Delta \int R(\epsilon)d\epsilon$	Position of DOS Centre (between 0eV to -3eV ) $E$ (eV)
Ag	-4.61	0	3.83	0	-2.47
Ag <sub>75</sub> In <sub>25</sub>	-4.65	0.04	2.94	-0.89	-2.50
Ag <sub>75</sub> Co <sub>25</sub>	-4.35	0.26	10.46	6.63	-1.84
Ag <sub>75</sub> Fe <sub>25</sub>	-4.42	0.19	8.46	4.63	-1.90
Ag <sub>75</sub> Cu <sub>25</sub>	-4.49	0.12	10.12	6.29	-1.90

\* $\epsilon$  is the binding energy;  $R(\epsilon)$  is the intensity of DOS.





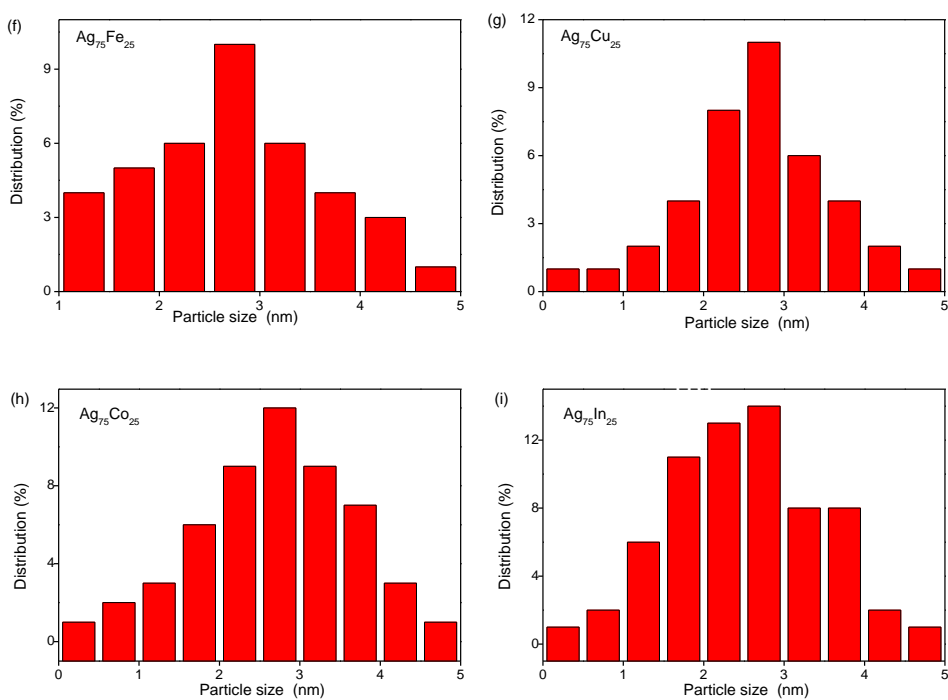
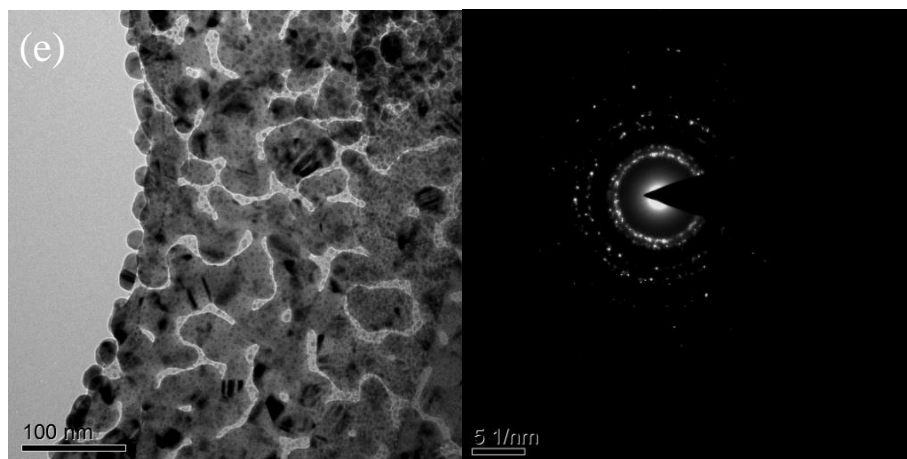


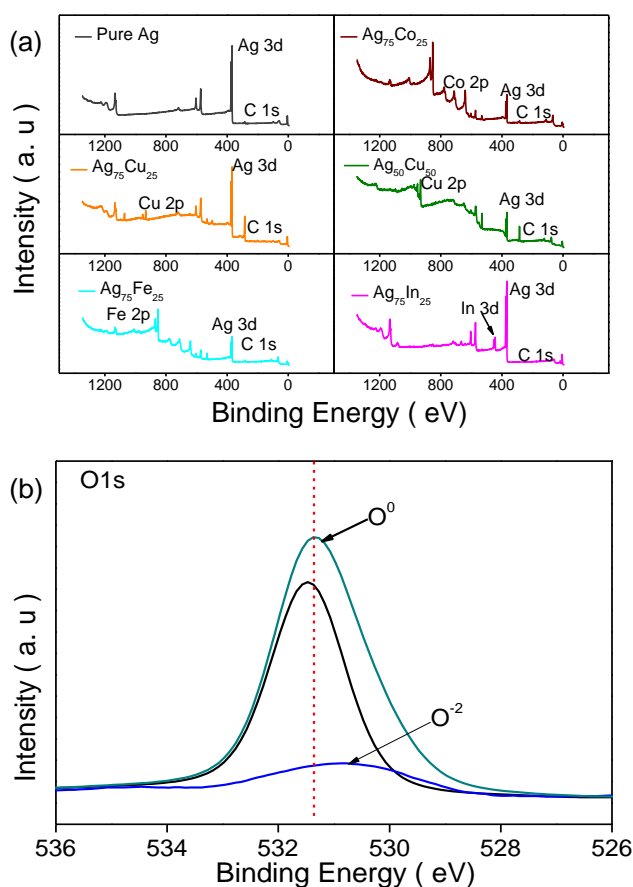
**Figure S7.** TEM images and selected area diffraction patterns (SAED) of the Ag-M alloys, (a)  $\text{Ag}_{75}\text{Fe}_{25}$ , (b)  $\text{Ag}_{75}\text{In}_{25}$ , (c)  $\text{Ag}_{75}\text{Co}_{25}$ , (d)  $\text{Ag}_{50}\text{Cu}_{50}$ , (e) Pure Ag, (f - i) particle size distribution of the Ag-M catalysts corresponding to TEM images.



1  
2 **Part 5. XPS results of Ag-M catalyst**

3 **Surface electronic structure properties**

4  
5 X-ray photoelectron spectroscopy (XPS) measurements were performed on an  
6 ULTRA (ESCALAB 250, Al  $K\alpha$ , ultrahigh vacuum is  $10^{-9}$ ,  $h\nu = 1486.6$  eV ). The  
7 data obtained is the typically of the samples. High-resolution O1s, Cu2p and Ag3d  
8 spectra were acquired. No charge compensation was necessary. The origin of the  
9 binding energy  $E_b$  was set to the Fermi energy  $E_f$  of the Au plate. The Shirley  
10 background is subtracted from the measured spectra. The d-band center of the valence  
11 band (VBS) is given by  $\int R(\epsilon)\epsilon d\epsilon / \int R(\epsilon) d\epsilon$ , in this work, the  $R(\epsilon)$  is the XPS-intensity  
12 (DOS-intensity) after background subtraction.<sup>[5]</sup>  
13  
14  
15



47 **Figure S8.** (a) Full survey scan XPS after Ar ion etching for the Ag, Ag<sub>75</sub>Co<sub>25</sub>, Ag<sub>75</sub>Cu<sub>25</sub>,  
48 Ag<sub>50</sub>Cu<sub>50</sub>, Ag<sub>75</sub>Fe<sub>25</sub> and Ag<sub>75</sub>In<sub>25</sub> samples. (b) O<sub>1s</sub> region in Ag-M alloys.  
49  
50  
51  
52  
53  
54  
55  
56  
57  
58  
59  
60  
61  
62  
63  
64  
65

**Part 6. Long-term stability analysis**

Long-term stability of the Ag<sub>75</sub>Cu<sub>25</sub> catalysts was assessed by accelerated testing, which was applied to the catalyst films in the same rotating disc electrode setup. The ORR curves at 1600 rpm, were recorded after 100, 600, 1000, 2000, 3000, 4000, 5000, 6000, 7000, 8000 and 9000 cycles. The Pb-stripping measurements was not performed at different cycle stage for one sample because we noted that the Pb- stripping measurements would pollute the catalyst surface, as shown in Figure S8c.<sup>[1]</sup> Hence, we prepared 14 different samples, in similar conditions, and performed the long-term stability test for each pattern in same way by measuring the ORR polarization curve of Ag<sub>75</sub>Cu<sub>25</sub> alloys after different cycles.

**Table S3.** Comparisons of Pb-stripping area, surface charge and ECSA of Ag<sub>75</sub>Cu<sub>25</sub> alloy after 100, 600, 1000, 2000, 3000, 4000, 5000, 6000, 7000, 8000 and 9000 cycles accelerated stability test.

Catalyst	Area of Pb-stripping (A)	Surface charge (Q <sub>h</sub> )	ECSA	Change of ECSA relative to the first cycle $\Delta ECSA$
	$\int j(E)dE/V$	$\times 10^6 \text{ uC/g}_{Ag}$	$\text{m}^2/\text{g}_{Ag}$	$\text{m}^2/\text{g}_{Ag}$
1	554.0	46.16	16.49	0
100	553.73	46.14	16.48	-0.01
600	551.38	45.95	16.41	-0.08
1000	547.94	45.66	16.30	-0.11
2000	541.02	45.09	16.10	-0.39
3000	535.84	44.65	15.95	-0.54
4000	527.50	43.96	15.70	-0.79
5000	520.07	43.34	15.47	-1.02
6000	511.68	42.64	15.22	-1.27
7000	505.81	42.15	15.05	-1.44
8000	493.94	41.16	14.70	-1.79
9000	478.42	39.87	14.24	-2.25

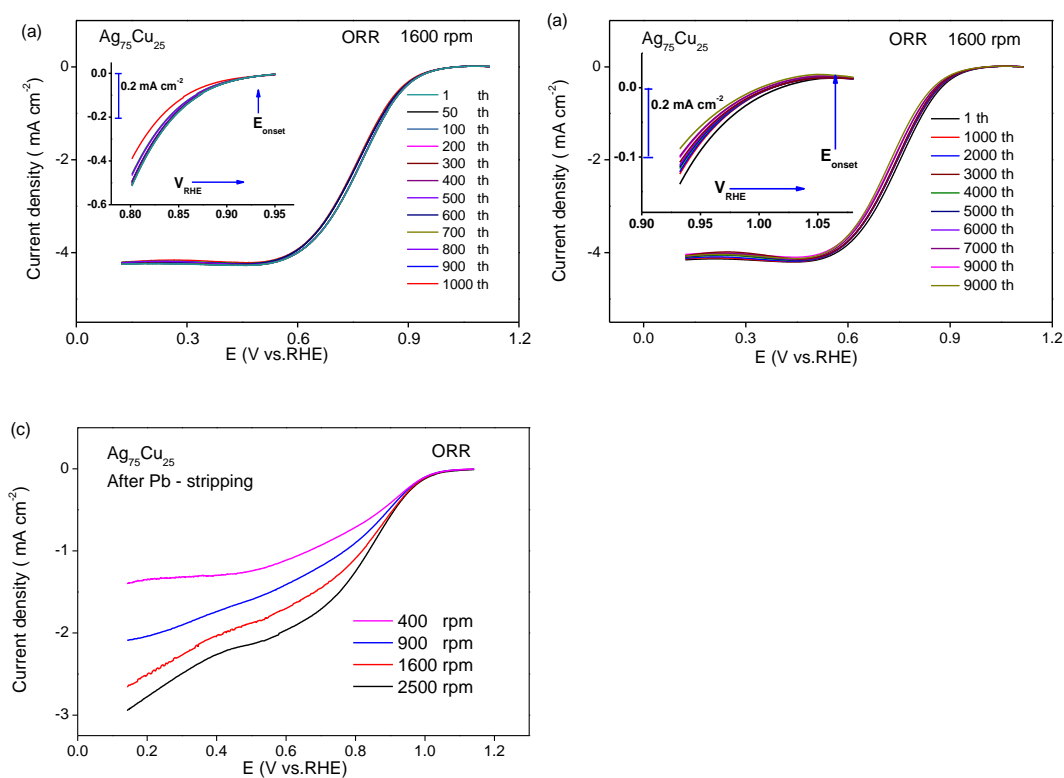


**Figure S9.** (a-b) The ORR polarization curves of  $\text{Ag}_{75}\text{Cu}_{25}$  alloy after 100, 600, 1000, 2000, 3000, 4000, 5000, 6000, 7000, 8000 and 9000 cycles. (c) the ORR polarization curve of  $\text{Ag}_{75}\text{Cu}_{25}$  alloy after Pb-stripping voltammetry test.

## References

1. A. Holewinski; J.C. Idrobo; S. Linic, *Nat. Chem.* **2014**, *6*, 828-34.
2. a) F.J. Vidal-Iglesias; J. Solla-Gullon; V. Montiel; A. Aldaz, *Electrochem. Commun.* **2012**, *15*, 42-45; b) J. Masa; C. Batchelor-McAuley; W. Schuhmann; R.G. Compton, *Nano Res.* **2014**, *7*, 71-78.
3. Y.Y. Liu; H.L. Jiang; Y.H. Zhu; X.L. Yang; C.Z. Li, *J. Mater. Chem. A* **2016**, *4*, 1694-1701.
4. E. Kirowa-Eisner; D. Tzur; E. Gileadi, *J. Electroanal. Chem.* **2008**, *621*, 146-158.
5. S.J. Hwang; S.K. Kim; J.G. Lee; S.C. Lee; J.H. Jang; P. Kim; T.H. Lim; Y.E. Sung; S.J. Yoo, *J. Am. Chem. Soc.* **2012**, *134*, 19508-11.